ORIGINAL PAPER

ANALYSIS OF POSITION COORDINATE ACCURACY OF TRIPLE GNSS SYSTEM BY POST-PROCESSING DUAL FREQUENCY OBSERVATIONS USING OPEN SOURCE GAMP: A CASE STUDY

Jabir Shabbir MALIK [1) *], **Zhang JINGRUI** [1)] **and Zahid Younas KHAN** [2, 3)]

[1)] *School of Aerospace Engineering, Beijing Institute of Technology, 100081 Beijing, China*
[2)] *School of Computer Science and Technology, Beijing Institute of Technology, 100081 Beijing, China*
[3)] *Department of Computer Science and Information Technology, University of Azad Jammu and Kashmir, Muzaffarabad, Pakistan*

Corresponding author's e-mail: jsmalik@bit.edu.cn

ARTICLE INFO

ABSTRACT

Multi GNSS system increases the GNSS positioning accuracy, efficiently improve the satellite geometry strength and further enhances precise point positioning (PPP) performance. In this study, positioning coordinate accuracy of GPS, GLONASS, Galileo and BeiDou dual frequency observations is estimated and comparatively analysed. Ten days of dataset from nine International GNSS service sites are adopted for eight different GNSS PPP scenarios. Position in east, north and up components and convergence speed test for single system GPS, GLONASS, BeiDou and Galileo, dual system GPS/GLONASS and Galileo/BeiDou, combined triple system GPS/GLONASS/BeiDou and GPS/GLONASS/Galileo is investigated. Results demonstrate that PPP solutions of GPS show an improvement in east, north and up components over GLONASS, BeiDou and Galileo PPP solutions. GPS PPP solutions reach to 2.88, 2.32 and 6.10 cm in east north and up components, respectively. Difference of standard deviation (STD) values between GPS and GLONASS PPP results is 4, 3 and 2 cm, in east, north and up direction, respectively. Moreover, difference of STD between GPS and Galileo PPP is >1cm in all three components. Furthermore, BeiDou only PPP results reach to 15, 10 and 20 cm in east, north and up direction in Asia Pacific, respectively. Horizontal component for combine Galileo/BeiDou PPP and GPS/GLONASS PPP solutions reach to 3.24 and 3.02 cm, respectively. Calculation results of 3D positioning show that combined GPS/GLONASS/BeiDou PPP solutions improve by 5.59 % and 17.72 % over GPS/GLONASS and Galileo/BeiDou PPP solutions, respectively. Furthermore, STD for 3D positioning of triple system GPS/GLONASS/Galileo shows an improvement of 47.53 %, 31.56 % and 24.90 % over Galileo/BeiDou, GPS/GLONASS and GPS/GLONASS/BeiDou PPP results, respectively. Two different convergence time tests are undertaken. Results of GPS-only PPP solutions show fastest convergence speed to achieve accuracy level of 1.0 cm over GLONASS-only, BeiDou-only, Galileo-only, and Galileo/BeiDou PPP solutions. Combine dual system GPS/GLONASS PPP convergence time show an improvement of 56.46 % over GPS-only solutions. The contribution of BeiDou to reducing the convergence time of the combine GPS/GLONASS PPP improve by 27.53 % over combine GPS/GLONASS PPP convergence time. Moreover, GPS/GLONASS/Galileo PPP convergence speed show an improvement of 20.06 % over convergent sessions of GPS/GLONASS/BeiDou PPP. Furthermore, to achieve accuracy level of 5.0 cm, combine three system GPS/GLONASS/BeiDou PPP reduces the convergence time than the GPS/GLONASS/Galileo convergent sessions length.

1. INTRODUCTION

Precise point positioning (PPP) is a most popular positioning technique among GNSS users due to its high accuracy and flexibility. As a result, PPP attracted wide attention within GNSS research community. PPP employs precise satellite orbit and clock products generate by the International GNSS Service (IGS) to improve the positioning accuracy (Zumberge et al., 1997; Kouba and Héroux, 2001). The improvement of positioning accuracy and initialization time that required to converge position accuracy from decimeter to centimeter are two most critical parts in PPP (Cai and Gao, 2015). Researchers and scientists utilize GNSS data for scientific research and GNSS applications, such as landslide monitoring (Wang, 2013; Capilla et al., 2016), crustal deformation (Tadokoro et al., 2012), meteorological applications (Li et al., 2015; Acheamponget al., 2016), GNSS-reflectometry applications (Malik et al., 2018) and surface tomographic studies (Dong and Jin, 2018). Modernization of European satellite system (Galileo) and the evolution of Chinese navigation system (BeiDou), integration of GPS, GLONASS, Galileo and BeiDou constellation significantly improve the positioning accuracy due to the increased number of available satellites (Montenbruck et al., 2017; Liu et al., 2017; Afifi and El-Rabbany, 2016). To achieve better positioning accuracy, error source such as ionospheric delay must be mitigated. Therefore, PPP models such as ionospheric-free (IF) linear

combinations to remove ionosphere first order delay or un-differenced un-combined (UDC) model by using parameter estimation is adopted to mitigate the ionospheric delay (Zhou et al., 2018a). UDC model is considered as a multi-frequency PPP model that keeps all the basic information of the observation and avoid noise amplification (Liu et al., 2017; Liu et al., 2019). Next generation GPS III block system has successfully completed the in-orbit check after August 2019 (http://www.gps.gov). GLONASS system recently introduced the Code Division Multiple Access (CDMA) signals, while keeping the Frequency Division Multiple Access (FDMA) signals and the improvement of the on-board clock stability (http://www.glonass-iac.ru). At the end of 2020 or beginning of 2021, Galileo system will be upgraded the constellation from 24 to 26 operational satellites (also included In-Orbit Validation (IOV) three satellites). Old commercial service will be replaced by a High-Accuracy Service (HAS) and a Commercial Authentication Service (CAS). Currently, Galileo system is transmitting signals on five frequencies, i.e. E1 (1575.42 MHz), E5a (1176.45 MHz), E5b (1207.14 MHz), E5 (1191.795 MHz) and E6 (1278.75 MHz) for several public services (Liu et al., 2019). Recently, 30th BD-3 satellite was launched into geosynchronous orbit and currently BeiDous system comprises total of 55 satellites in orbit (www.en.beidou.gov.cn). BeiDous satellite based augmentation system (BDSBAS) provides services, among others, in aerospace, maritime affairs, transportation, and agriculture industry (Li et al., 2020; Hein, 2020).

Several PPP software packages have been developed by different research and academic organizations. Bernese is a commercial software developed at Astronomical Institute of the University of Bern (AIUB) (Dach et al., 2009). Bernese software handles single and dual frequency GPS and GLONASS observations. GIPSY/OASIS (GOA II) designed and developed by National Aeronautical and Astronautical Jet Propulsion Laboratory (NASA, JPL) (https://gipsy-oasis.jpl.nasa.gov/gipsy/index.php), process GPS dual frequency observations and provides station coordinates, clock offsets and estimates of atmospheric products. The ''GPS Toolkit'' (GPSTk) is an open source project developed by the Applied Research Laboratories of the University of Texas (ARL, UT) (Salazar et al., 2010). GPSTk consists of core library, mathematical functions, and source codes for GNSS community. GAMIT/GLOBK developed by Massachusetts Institute of technology (MIT), which is a comprehensive analysis packages for GPS observations. Output of GAMIT contains 3- dimensional relative positioning and earth-rotation parameters (Herring et al., 2015). GNSS-Lab (gLAB) is developed by Astronomy and Research Group at Universitat Politecnica de Catalunya (UPC) is a multipurpose programming tool suit to process

single and dual frequency of GPS and GLONASS measurements (Hernandez-Pajares et al., 2010). PPPH is an open software package, built and designed onto popular programming language MATLAB (Bahadur and Nohutcu, 2018). PPPH is implemented for analyzing dual frequency precise point positioning single or combined GNSS system (GPS, GLONASS, Galileo and BeiDou). Extra visual components and tools must be installed for MATLAB 2016a or older versions. Aforementioned software tools and packages design on different programming languages. In addition, all of the software packages have complex data structure and complicated modules to process GNSS measurements. Moreover, some commercial software requires an official license and payment fees for registration.

The performance of the GPS-only and combined GPS/GLONASS PPP has been widely investigated, which confirms the improvements in the accuracy and convergence time (Martín et al., 2011; Cai and Gao, 2013; Choy et al., 2013; Yigit et al., 2014; Malik, 2020). In some studies performance assessment of GPS-only and combined GPS/BeiDou PPP was analysed (Wang et al., 2017). Shi et al. (2012) analyzed BeiDous/GPS combined PPP solutions using PANDA (Position and Navigation Data Analyst, developed by the GNSS Research Center at Wuhan University) software package. The RMS of static PPP can reach several centimeters to even millimeters for baseline relative positioning. Zhao et al. (2017) showed that the contribution of BeiDou observations to the combined GPS/GLONASS PPP in Asia-Pacific region significantly reduces mean convergence speed by an average of 49.6 % with short observations of data and under harsh environment. The Galileo constellation further increases the number of visible satellites and enhances geometric structure in space (Xia et al., 2019). Afifi and El-Rabbany (2016) demonstrated that the combination of Galileo, BeiDou and GPS observations further increased the positioning accuracy and shortens the convergence time compared to the GPS static PPP solutions. Xia et al. (2019) indicated that combination of Galileo, GPS and GLONASS observations can be improved by 11.03 %, 10.59 % and 11.07 % in the north, east and up components in static mode, respectively. The average convergence time can be reduced by 11.04 % for GPS/GLONASS solutions by adding Galileo observations. Liu et al. (2019) analyzed combined GPS/Galileo/BeiDou PPP with ambiguity resolution (PPP-AR) and estimated fractional cycle biases (FCB) for GPS, Galileo and BeiDou system using PANDA software. Their results show that combined GPS/Galileo/BDS PPP results can be improved in east and north components. For the cut-off elevation angle of 40^0, the use of combine three system GPS/GLONASS/Galileo enable to obtain about 90 % of the availability of PPP solutions with a centimeter-level accuracy (Kiliszek and Kroszczyński, 2020). In Ogutcu (2020), PPP solutions are analyzed using three

different cut-off angles 5^0, 15^0 and 30^0, static PPP results show that three-dimensional accuracy is improved when adding Galileo to GPS/GLONASS static PPP, especially for short observation times and up to 50 % (12 hr) and 65 % (24 hr) improvements are observed for horizontal and vertical components, respectively.

Previous studies demonstrated that with the addition of Galileo observations with combined GPS/GLONASS PPP solutions provide better position accuracy and reduce the convergence time. In addition, BeiDou system has been announced globally after June 2020. Therefore, main motivation of this research is to evaluate and comparative analyze the static PPP coordinates accuracy and convergence speed test of single-, dual- and triple system. Primary focus of this study is the post-processing the GNSS data observations from each of the GNSS constellation (GPS, GLONASS, BeiDou, and Galileo). In addition, this study also investigates the positioning estimates achievable using integration of Galileo and BeiDou observations to the combine GPS/GLONASS PPP results using recently available open source software GAMP for GPS (G), GLONASS (R), BeiDou (C), Galileo (E), combined two system GPS/GLONASS (G/R), Galileo/BeiDou (E/C) and three system GPS/GLONASS/BeiDou (G/R/C) and GPS/GLONASS/Galileo (G/R/E) PPP combinations.

2. MULTI GNSS PPP MODELLING

The basic observation equations for GNSS pseudorange (P) and carrier phase (L) can be expressed as (Zhou et al., 2018b; Lou et al., 2016);

$$P_{f,r}^j = \rho_r^j g + \delta t_r - \delta T^j + c(d_{f,r} - d_f^j) + I_{f,r}^j + m_r^j Z_r + \xi(P_{f,r}^j) \tag{1}$$

$$L_{f,r}^j = \rho_r^j g + \delta t_r - \delta T^j + \lambda_f(\ell_{f,r} - \ell_f^j) - I_{f,r}^j + N_{f,r}^j \lambda_f + m_r^j Z_r + \xi(L_{f,r}^j) \tag{2}$$

$$I_{f,r}^j = \chi_f I_{f,r}^j \; ; \; \chi_f = \lambda_f^2/\lambda_1^2 \tag{3}$$

where scripts f, r, and j shows the frequency of satellite ($f = 1$, 2), receiver, and satellite system respectively; ρ_r^j is the true geometric range between satellite and the receiver, c is the speed of light in vacuum (m/s); δt_r and δT^j are the receiver and satellite clock offset in seconds, respectively; $d_{f,r}$ and d_f^j are un-calibrated code bias (UCB) of the receiver and satellite; $\ell_{f,r}$ and ℓ_f^j are the un-calibrated phase delay (UPD) of the receiver and satellite; $I_{f,r}^j$ is the ionospheric delay of the signal in meters; $N_{f,r}^j$ is the integer carrier phase ambiguity term in cycle; λ_f^j is the carrier wavelength of dual frequency in meters; χ_f is the frequency dependent multiplier factor; Z_r tropospheric zenith wet delay; m_r^j is the wet mapping function; $\xi(P_{f,r}^j)$

and $\xi(L_{f,r}^j)$ are un-modelled measurement errors (noise, multipath) in GNSS code and phase observations respectively. The slant tropospheric delay on the path can be split into a hydrostatic dry part (ZHD) and a non-hydrostatic wet part (ZWD). ZHD is modelled using empirical Saastamoinen model (Saastamoinen, 1972); While, ZWD is estimated as unknowns along with other parameters in PPP model. Traditionally, ionospheric free (IF) linear combination of pseudo-range and phase observations is adopted to remove the ionospheric delay, however, in this study uncombined pseudorange and carrier phase observation model is used to estimate the slant ionospheric delay as unknown parameter. Therefore, linearizing Eq(1) and Eq(2), we get;

$$p_{f,r}^j = -\boldsymbol{u}_r^j \cdot \boldsymbol{v}_r + \delta t_r - \delta T^j + c(d_{f,r} - d_f^j) + \chi_f I_{f,r}^j + m_r^j Z_r + \xi(P_{f,r}^j) \tag{4}$$

$$l_{f,r}^j = -\boldsymbol{u}_r^j \cdot \boldsymbol{v}_r + \delta t_r - \delta T^j + \lambda_f(\ell_{f,r} - \ell_f^j) + N_{f,r}^j \lambda_f - \chi_f I_{f,r}^j + m_r^j Z_r + \xi(L_{f,r}^j) \tag{5}$$

where $p_{f,r}^j$ and $l_{f,r}^j$ denotes observed minus computed (OMC) pseudorange and phase observables from satellite j to receiver r at the frequency f, with all the necessary corrections i.e, satellite and receiver antenna phase center offsets (PCO) and variations (PCVs), relativistic effects, Sagnac effect, tidal loadings, and phase windup is already modeled and added; $\boldsymbol{u}_r^j$ is the unit vector of the direction from receiver to satellite; $\boldsymbol{v}_r$ denotes the vector of the receiver position increments relative to a priori position for linearization. For the multi GNSS constellation (GPS/GLONASS/Galileo/BeiDou) PPP model of the pseudorange and carrier phase can be expressed as

$$\begin{cases} p_{f,r}^G = -\boldsymbol{u}_r^G \cdot \boldsymbol{v}_r + \delta t_r - \delta T^G + c(d_{G,r} - d_f^G) + \\ \quad\quad + \chi_G I_{f,r}^G + m_r^G Z_r + \xi(P_{f,r}^G) \\ p_{f,r}^{R_j} = -\boldsymbol{u}_r^R \cdot \boldsymbol{v}_r + \delta t_r - \delta T^R + c(d_{R_j,r} - d_f^R) + \\ \quad\quad + \chi_{R_j} I_{f,r}^R + m_r^R Z_r + \xi(P_{f,r}^G) \\ p_{f,r}^C = -\boldsymbol{u}_r^C \cdot \boldsymbol{v}_r + \delta t_r - \delta T^C + c(d_{C,r} - d_f^C) + \\ \quad\quad + \chi_C I_{f,r}^C + m_r^C Z_r + \xi(P_{f,r}^C) \\ p_{f,r}^E = -\boldsymbol{u}_r^E \cdot \boldsymbol{v}_r + \delta t_r - \delta T^E + c(d_{E,r} - d_f^E) + \\ \quad\quad + \chi_E I_{f,r}^E + m_r^E Z_r + \xi(P_{f,r}^G) \end{cases} \tag{6}$$

$$\begin{cases} l_{f,r}^G = -\boldsymbol{u}_r^G \cdot \boldsymbol{v}_r + \delta t_r - \delta T^G + \lambda_G(\ell_{G,r} - \ell_f^G) + \\ \quad\quad + N_{f,r}^G \lambda_G - \chi_G I_{f,r}^G + m_r^G Z_r + \xi(L_{f,r}^G) \\ l_{f,r}^{R_j} = -\boldsymbol{u}_r^R \cdot \boldsymbol{v}_r + \delta t_r - \delta T^R + \lambda_{R_j}(\ell_{R_j,r} - \ell_f^R) + \\ \quad\quad + N_{f,r}^R \lambda_{R_j} - \chi_{R_j} I_{f,r}^R + m_r^R Z_r + \xi(L_{f,r}^R) \\ l_{f,r}^C = -\boldsymbol{u}_r^C \cdot \boldsymbol{v}_r + \delta t_r - \delta T^C + \lambda_C(\ell_{C,r} - \ell_f^C) + \\ \quad\quad + N_{f,r}^C \lambda_C - \chi_C I_{f,r}^C + m_r^C Z_r + \xi(L_{f,r}^C) \\ l_{f,r}^E = -\boldsymbol{u}_r^E \cdot \boldsymbol{v}_r + \delta t_r - \delta T^E + \lambda_E(\ell_{E,r} - \ell_f^E) + \\ \quad\quad + N_{f,r}^E \lambda_E - \chi_E I_{f,r}^E + m_r^E Z_r + \xi(L_{f,r}^E) \end{cases} \tag{7}$$

where superscripts G, R, C and E refer to the GPS, GLONASS, BeiDou and Galileo, respectively; R_j

denotes the GLONASS satellite with frequency factor *j* that are used for the computation of the carrier phase frequencies of the individual GLONASS satellites; $\textit{\char'46}_{G,r}$, $\textit{\char'46}_{R,r}$, $\textit{\char'46}_{C,r}$ and $\textit{\char'46}_{E,r}$ denotes phase delays of the receiver *r* for *G*, *R*, *C* and *E*, respectively; $d_{G,r}$, $d_{R,r}$, $d_{C,r}$ and $d_{E,r}$ refers to the UCBs of the receiver for *G, R, C* and *E*, respectively.

Frequency dependent satellite differential code bias (DCB) between pseudoranges of different GNSS constellation needs to be corrected using products from Center for Orbit Determination in Europe (CODE). The receiver UCBs are identical for code-division multiple access (CDMA) signals (i.e., GPS, BeiDous, and Galileo) for all the satellites at each frequency, while they are different for GLONASS due to the frequency division multiple access (FDMA) technique, which lead to frequency-dependent biases in the receiver (Liu et al., 2017). For the GLONASS satellites with different frequency factors, the receiver code biases are different. These biases are referred to as inter-channel or inter-frequency biases (ICBs/IFBs), these bianes will influence positioning and show up in code residuals if not considered. GLONASS code IFBs are modeled as satellite-specific or frequency-specific parameters in PPP model. Both the ionospheric delay and DCBs are frequency dependent. This implies that not all parameters can be unbiasedly estimable due to rank deficiency. Ionospheric delay and receiver DCB are perfectly correlated, and they are estimated as lumped terms.

In multi GNSS PPP approach, precise satellite orbit and clock products provide by international GNSS service (IGS) multi GNSS Experiment (MGEX) are applied, resulting satellite clock offsets absorb satellite UCBs in pseudorange Eq(6) and carrier phase Eq(7) ;

$$
\begin{cases}
p_{f,r}^G = -\boldsymbol{u}_\mathbf{r}^\mathbf{G} \cdot \boldsymbol{v}_\mathbf{r} + \delta t_r + c\big(d_{G,r}\big) + \\
\quad + \chi_G I_{f,r}^G + m_r^G Z_r + \xi\big(P_{f,r}^G\big) \\
p_{f,r}^{R_j} = -\boldsymbol{u}_\mathbf{r}^\mathbf{R} \cdot \boldsymbol{v}_\mathbf{r} + \delta t_r + c\big(d_{R_j,r}\big) + \\
\quad + \chi_{R_j} I_{f,r}^R + m_r^R Z_r + \xi\big(P_{f,r}^G\big) \\
p_{f,r}^C = -\boldsymbol{u}_\mathbf{r}^\mathbf{C} \cdot \boldsymbol{v}_\mathbf{r} + \delta t_r + c\big(d_{C,r}\big) + \\
\quad + \chi_C I_{f,r}^C + m_r^C Z_r + \xi\big(P_{f,r}^C\big) \\
p_{f,r}^E = -\boldsymbol{u}_\mathbf{r}^\mathbf{E} \cdot \boldsymbol{v}_\mathbf{r} + \delta t_r + c\big(d_{E,r}\big) + \\
\quad + \chi_E I_{f,r}^E + m_r^E Z_r + \xi\big(P_{f,r}^G\big)
\end{cases}
$$

$$
\begin{cases}
l_{f,r}^G = -\boldsymbol{u}_\mathbf{r}^\mathbf{G} \cdot \boldsymbol{v}_\mathbf{r} + \delta t_r + \lambda_G\big(\textit{\char'46}_{G,r} - \textit{\char'46}_f^G\big) + \\
\quad + N_{f,r}^G \lambda_G - \chi_G I_{f,r}^G + m_r^G Z_r + \xi\big(L_{f,r}^G\big) \\
l_{f,r}^{R_j} = -\boldsymbol{u}_\mathbf{r}^\mathbf{R} \cdot \boldsymbol{v}_\mathbf{r} + \delta t_r + \lambda_{R_j}\big(\textit{\char'46}_{R_j,r} - \textit{\char'46}_f^R\big) + \\
\quad + N_{f,r}^R \lambda_{R_j} - \chi_{R_j} I_{f,r}^R + m_r^R Z_r + \xi\big(L_{f,r}^R\big) \\
l_{f,r}^C = -\boldsymbol{u}_\mathbf{r}^\mathbf{C} \cdot \boldsymbol{v}_\mathbf{r} + \delta t_r + \lambda_C\big(\textit{\char'46}_{C,r} - \textit{\char'46}_f^C\big) + \\
\quad + N_{f,r}^C \lambda_C - \chi_C I_{f,r}^C + m_r^C Z_r + \xi\big(L_{f,r}^C\big) \\
l_{f,r}^E = -\boldsymbol{u}_\mathbf{r}^\mathbf{E} \cdot \boldsymbol{v}_\mathbf{r} + \delta t_r + \lambda_E\big(\textit{\char'46}_{E,r} - \textit{\char'46}_f^E\big) + \\
\quad + N_{f,r}^E \lambda_E - \chi_E I_{f,r}^E + m_r^E Z_r + \xi\big(L_{f,r}^E\big)
\end{cases}
$$

An equation to estimate unknown parameters in a state space vector V can be written as (Liu et al., 2017);

$$ V = \big(\boldsymbol{v}_\mathbf{r}\ \delta t_r\ d_{R,r}\ d_{C,r}\ d_{E,r}\ I_r^j\ Z_r\ \widetilde{N}_r^j\big)^T $$

$$ \widetilde{N}_r^j = N_r^j + \textit{\char'46}_r + \textit{\char'46}_f^j $$

The vector *V* includes, the receiver position increment $\boldsymbol{v}_\mathbf{r}$, receiver clock offset δt_r, zenith tropospheric wet delay Z_r, slant ionospheric delay I_r^j, phase ambiguity $\widetilde{N}_r^j$ in which UPD will be absorbed by phase ambiguity term, and the frequency dependent UCBs in the receiver $d_{R,r}\ d_{C,r}\ d_{E,r}$ relative to the GPS $d_{G,r}$. The estimated parameters can be smoothed through a forward and backward filtering in post-processing mode. To get most strengthen PPP solutions, priori knowledge of the ionospheric delays including the temporal correlation, spatial characteristics and external ionospheric model is also utilized to constrain the estimated ionospheric parameters. These constraints, to be imposed on observations of a single station can be expressed as

$$ I_{r,k}^j - I_{r,k-1}^j = x_k, x_k \approx N(0, \sigma_{xk}^2) $$

$$ vI_r^j = \frac{I_r^j}{f_{r,IPPP}^j} = a_0 + a_1 dL + a_2 dL^2 + a_3 dB + a_4 dB^2, \sigma_{vl}^2 $$

$$ I_r^j = \tilde{I}_r^j, \sigma_I^2 $$

where *k* is the current epoch and *k–1* is the previous epoch; x_k is a zero mean with variance σ_{xk}^2; vI_r^j is the vertical ionospheric delay with a variance σ_{vl}^2; $f_{r,IPPP}^j$ is the mapping function at the ionospheric pierce point (IPP); the coefficients a_i describe the trend; dL and dB are the longitude and latitude difference between the IPP and the station location; $\tilde{I}_r^j$ is the ionospheric delay obtained from external ionospheric model with a variance of σ_I^2.

3. PERFORMANCE ANALYSIS AND METHODOLOGY

3.1. EXPERIMENT SITE

Consecutive ten days of dataset is collected from 9 IGS stations which are distributed around the Earth during September 21 – 30, 2020. IGS sites are also designated as MGEX stations which are equipped with multi- GNSS receivers to instantaneously track observations from GPS, GLONASS, Galileo and BeiDou satellites. Figure 1 presents the geographic location of IGS stations adopted in this study. Table 1 shows the IGS study sites, coordinates, receiver type and antenna. Figure 2 shows IGS station mean number of available GNSS satellite system and the position dilution of precision (PDOP) values of different GNSS combinations mode, i.e., single system GPS (G-only), GLONASS (R-only), Galileo (E-only), BeiDou (C- only), combined dual system GPS/GLONASS (G/R) and Galileo/BeiDou (E/C), triple system
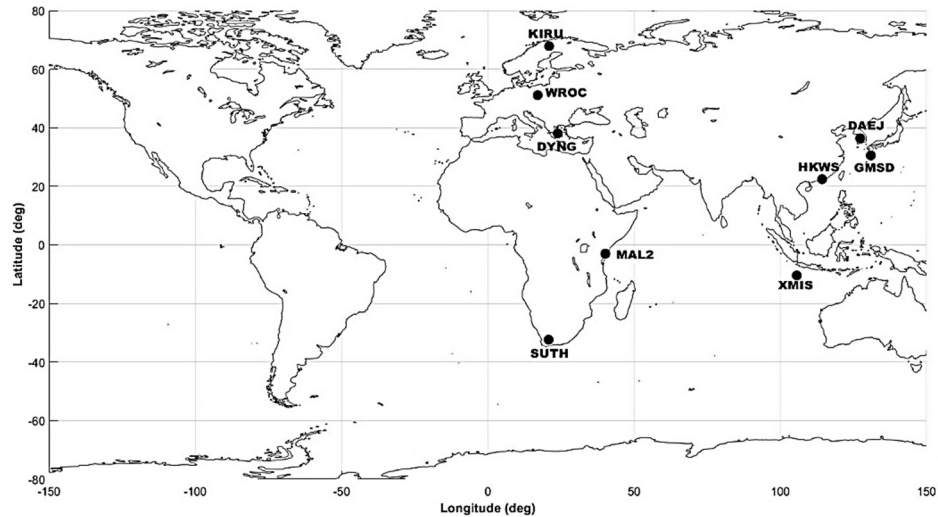
Fig. 1   Geographical distribution of IGS MGEX stations used in the study.

Table 1 Information about IGS MGEX stations coordinates, receiver and antenna type.

Site	Location	Coordinates (d:m:s)		Receiver	Antenna type	
		Latitude	Longitude			
WROC	Poland	51° 06′ 47.75″	17° 03′ 43.30″	LEICA GR50	LEIAR25.R4	LEIT
HKWS	Hong Kong	22° 26′ 03.42″	114° 20′ 07.36″	LEICA GR50	LEIAR25.R4	LEIT
MAL2	Kenya	−02° 59′ 45.60″	40° 11′ 38.01″	SEPT POLARX4	LEIAR25.R4	NONE
DAEJ	S. Korea	36° 23′ 57.90″	127° 22′ 28.10″	TRIMBLE NETR9	TRM59800.0	SCIS
KIRU	Sweden	67° 51′ 26.50″	20° 58′ 06.40″	SEPT POLARX5	SEPCHOKE_B3E6	SPKE
DYNG	Greece	38° 04′ 42.80″	23° 55′ 56.80″	TRIMBLE NETR9	TRM59800.0	NONE
SUTH	S. Africa	−32° 22′ 48.70″	20° 48′ 37.70″	SEPT POLARX5	ASH701945G_M	NONE
GMSD	Japan	30° 33′ 23.20″	131° 00′ 56.00″	TRIMBLE NETR9	TRM59800.0	NONE
XMIS	Australia	−10° 26′ 59.90″	105° 41′ 18.60″	TRIMBLE NETR9	JAVRINGANT_DM	NONE
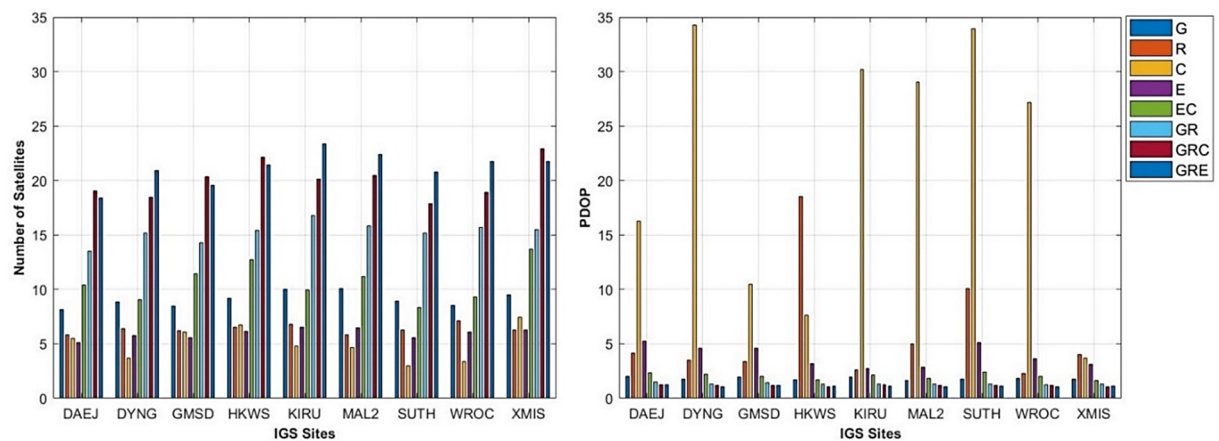
Fig. 2   Plot of average number of GNSS satellites and average PDOP values at each IGS stations.

GPS/GLONASS/BeiDou – (G/R/C) and GPS/GLONASS/Galileo – (G/R/E) PPP combinations. PDOP represent the quality of the satellite arrangements, geometric structure and satellites distribution (Pan et al., 2019). Analyzing Figure 2, it clearly shows that among single GNSS system, G-only system has more available number of satellites at each IGS stations. Minimum PDOP of G- only is 1.67 at MAL2. While, maximum PDOP of G-only system reaches to 2.03 at DAEJ. G-only system has maximum of 10.09 available satellites at MAL2. C-only system has different satellite distributions at different IGS sites and maximum satellites are tracked in Asia Pacific region i.e., at stations DAEJ, HKWS, GMSD and XMIS. In addition, PDOP of C-only system at DAEJ, HKWS,

GMSD and XMIS reaches to 16.27, 10.44, 7.64 and 3.69, respectively. Moreover, PDOP values for C-only system are relatively very high at stations DYNG, KIRU, SUTH and WROC, respectively. The higher PDOP value at these stations indicates poor geometry and arrangement of satellites for C-only system. Furthermore, R-only system has maximum 7.15 and minimum 5.81 number of GNSS satellites at WROC and MAL2 with the corresponding PDOP value is 2.27 and 5.01, respectively. In addition, PDOP for R-only system reaches to 18.53 and 10.01 at HKWS and SUTH respectively. On the other hand, E-only system has maximum of 6.57 and minimum of 5.09 GNSS satellites at KIRU and DAEJ respectively. It can be inferred from Figure 2 that the combined E/C and G/R system increases the distribution of satellites in the sky and consequently decreased the PDOP (values range within 1.66 to 2.45 for E/C system and 1.25 to 1.49 for G/R system). On the other hand, combined three systems G/R/C and G/R/E PPP further increased the number of available satellites and significantly reduced the PDOP in comparison with dual system E/C and G/R PPP mode. Minimum of 17.89 and maximum of 22.91 number of GNSS satellites available for G/R/C system at SUTH and XMIS, respectively. In addition, combined G/R/C mode has more availability of satellites than G/R/E PPP at DAEJ, GMSD, HKWS and XMIS stations. However, difference of PDOP values between G/R/C and G/R/E PPP mode at these mentioned sites are comparatively very small about 0.02.

Maximum number of 23.36 and minimum of 18.37 satellites are available for G/R/E PPP at stations KIRU and DAEJ, respectively. Furthermore, PDOP values of combined G/R/C and G/R/E system are the lowest at all the IGS sites than the G-only, R-only, E-only, C-only and the combined dual system G/R and E/C PPP combinations. Table 2 outlines the availability of the mean number of each GNSS satellites system and PDOP values of eight GNSS PPP combinations. Results are the mean number of observed satellites and PDOP during whole ten days of datasets. It can be illustrated from Table 2 that the GPS possess higher number of available satellites than the GLONASS, BeiDou and Galileo system and

Table 2 Average number of visible satellites and PDOP for different GNSS PPP combinations mode.

System	Average	
	Satellites	PDOP
GPS	9.08	1.83
GLONASS	6.36	5.95
Galileo	5.95	3.91
BeiDou	5.03	21.40
Galileo/BeiDou	10.67	2.05
GPS/GLONASS	15.26	1.34
GPS/GLONASS/BeiDou	20.03	1.17
GPS/GLONASS/Galileo	21.14	1.13

average PDOP is 1.83. Moreover, BeiDou system has higher PDOP values among single GNSS system. This is because average PDOP for BeiDou system is very high ~ (values range from 27 to 35) at DYNG, KIRU, SUTH MAL2 and WROC. With the integration of GLONASS and GPS system, the dual system yields increase availability of satellites and decreased the PDOP values. It is worth mentioning that GPS PDOP is improved over Galileo/BeiDou combined PPP mode. Therefore, integration of BeiDou system to the Galileo system only increases global distribution of visible satellites. Moreover, PDOP for the combined GPS/GLONASS PPP reduces to 1.34. Results from Table 2 show that higher number of GNSS satellites is available for the combined GPS/GLONASS/BeiDou and PS/GLONASS/Galileo PPP mode and the PDOP reach to 1.17 and 1.13, respectively.

3.2. PPP PERFORMANCE STRATEGY

All the 24 hour observations from GPS, GLONASS, Galileo and BeiDou system are sampled at 30s interval. In this study, open-source software GAMP (GNSS Analysis software for Multi-constellation and multi-frequency Precise positioning) is adopted (Zhou et al., 2018b). GAMP is a modification of RTKLIB (Takasu and Yasuda, 2009), which mainly focuses on the multi-GNSS (GPS, GLONASS, Galileo, BeiDou and QZSS) single point (SP) and precise point (PP) positioning. The source code can be accessed via the GPS Toolbox: https://www.ngs.noaa.gov/gps-toolbox/GAMP. In GAMP, cycle slips are detected in two different combinations i.e., Melbourne–Wübbena (MW) combination and the geometry-free (GF) combination. Typical threshold values are determined for the detection of cycle slips on GNSS measurements. GLONASS code IFBs can be handled in four different schemes, i.e., (1) ignoring IFBs, (2) modeling IFBs, (3) estimating IFBs for each GLONASS frequency, and (4) estimating IFBs for each GLONASS satellite (Zhou et al., 2018b). Table 3 shows the PPP processing strategy adopted for PPP solutions.

Station coordinates are considered as constant. The initial standard deviation values for the code and carrier phase is 0.3 m and 0.003 m for GNSS observations, respectively. For the BeiDou observations, measurement error ratio between carrier phase and code is set to 200, while measurement error ratio between carrier phase and code is 100 for each GPS, GLONASS and Galileo observations. The spectral densities for receiver clock offset and zenith tropospheric delay are set to 1.0×10^4 m^2/sec and 1.0×10^{-8} m^2/sec, respectively. Inter system biases (ISB) are considered as a time constant. The precise orbit and clock products provided by Center for Orbit Determination in Europe (CODE) (one of MGEX Analysis centers) with a sampling rate of 300 s and 30 s respectively are adopted for orbit and clock corrections, respectively. In order to analyze the PPP

Table 3 PPP performance analysis strategy.

GNSS constellation	GPS, GLONASS, Galileo and BeiDou
PPP mode	Static only
Observables	Un-differenced and un-combined (UDUC) dual frequency carrier phase and code observations
Satellite orbit and clock	Final precise MGEX products (CODE)
Satellite antenna phase MGEX values	GPS and GLONASS from IGS antenna model IGS14.atx, and conventional
center (PCOs/PCVs)	for BeiDou and Galileo constellation
Receiver antenna phase center (PCOs/PCVs)	IGS antenna model IGS14.atx, GPS values are used for Galileo and BeiDou
Differential code biases	P1–C1 and P2 – C2 (CODE Analysis center products)
Troposphere	
Dry component	Apriori values are used from Saastamoinen model
Wet component	Estimated using the Global Mapping Function: GMF
Estimator	Kalman Filter
Elevation mask	7^0
Weighting method	Elevation dependent weights $\{1/\sin(el)\}$
Priori observation	Carrier phase: 0.003 m and code pseudoranges: 0.3 m at zenith direction
GLONASS IFBs	Inter system Bias + Inter channel Bias for every satellite (ISB+ICB) for the combined PPP mode only
Solid earth tides, Phase wind up, Ocean tide loading, and Relativistic effect	Corrections applied (IERS 2010) (Petit et al., 2010)
Output analysis	Position (East, North, Up), 3D Positioning error, Tropospheric zenith total delay

performance, positioning accuracy in east, north and up direction is computed. Convergence time is computed after 24 hours data processing. Standard deviation (STD) is used as PPP performance indicator. STD values show the dispersion of PPP estimates w.r.t to IGS reference values in east, north and up direction. Values of STD can be considered the amount of error that occur in the PPP estimates. For the analysis of position accuracy, the dataset is processed in eight different PPP combinations. For the data post-processing Microsoft visual studio (VS15) is utilized in batch processing mode with the pre-requisite Python 2.7 installation. The precise coordinates of IGS stations are obtained from IGS Solution Independent Exchange format (SINEX) daily files. Table 4 outlines the IGS solution reference values in east, north and up components. IGS daily solutions are transformed from the geocentric earth-centered-earth-fixed (XYZ) coordinates into topocentric (ENU) coordinates system. All the estimates of the PPP results are referenced with the IGS SINEX daily combination of analysis centers (ACs) solutions, i.e., COD (Centre for Orbit Determination in Europe, Switzerland), ESA (European Space Agency, Germany), GFZ (Geoforschungszentrum, Potsdam, Germany), GRG (Groupe de Recherche en Geodesie Spatiale, Toulouse, France), JPL (Jet Propulsion Labs, Pasadena, California, U.S.A), MIT (Massachusetts Institute of Technology, U.S.A), NGS (National Geodetic Survey, U.S.A), NRC (Natural Resources Canada, Canada), and SIO (Scripps Institute of Oceanography, U.S.A).

Table 4 Reference values in east, north and up components from International GNSS Service (IGS) daily solutions (Unit: mm).

Sites	East	North	Up
DAEJ	0.20	−1.87	−7.81
DYNG	0.45	2.12	0.72
GMSD	0.40	-0.02	0.01
HKWS	0.83	0.26	2.42
KIRU	1.85	2.95	1.34
MAL2	2.74	-0.73	-1.31
SUTH	-1.80	-0.94	5.55
WROC	0.43	-0.01	0.95
XMIS	1.47	0.15	-1.45

4. RESULTS ANALYSIS AND DISCUSSION

In this section, positioning accuracy of eight different GNSS PPP combinations, namely, G–only, R–only, C–only and E–only, combined dual system G/R and E/C, triple system G/R/C and G/R/E PPP is investigated and analyzed. Statistical analysis is performed based on the performance metrics.

Figure 3 shows the number of GNSS satellites, PDOP values and positioning errors in east, north and up components for various GNSS PPP combinations at all IGS on day of the year (DOY) 269. It can be illustrated from Figure 3 that G-only PPP solutions best perform in east, north and up component at IGS sites on DOY 269 over R- only and C-only PPP solution. Similar PPP results are obtained for E-only system in east and north component with the exception
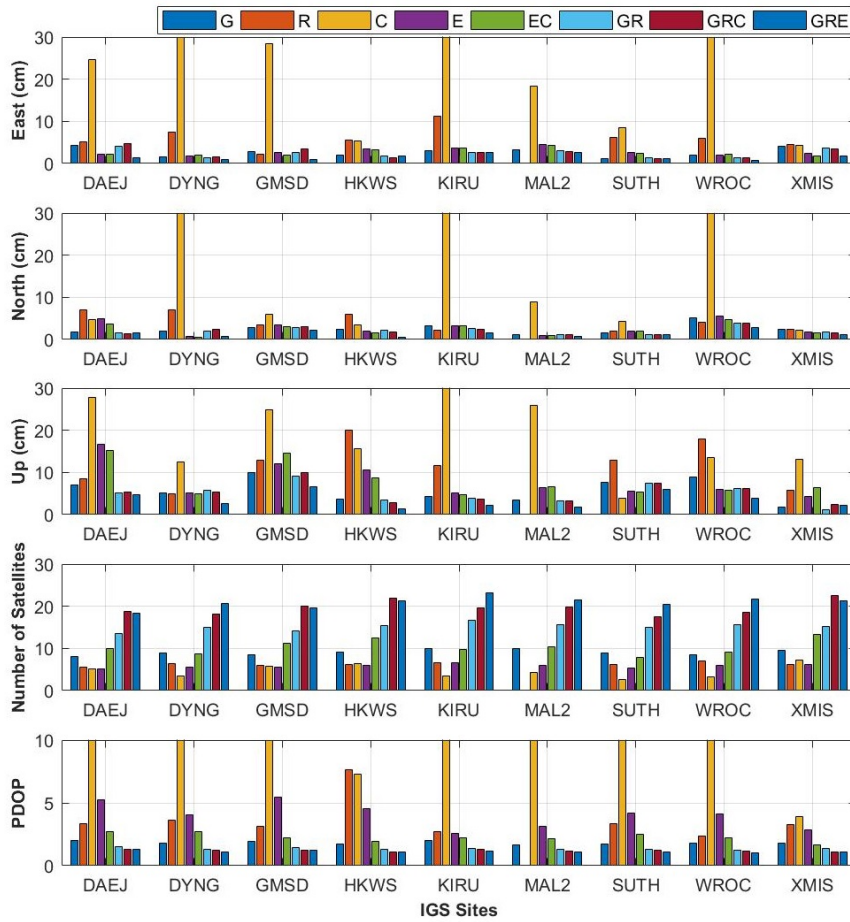
Fig. 3   Bar diagram of standard deviation (STD) in east, north and up components, number of GNSS satellites and PDOP at each IGS sites for single system (G, R, C, E), dual system (E/C, G/R), and triple system (G/R/C, G/R/E) PPP on DOY 269.
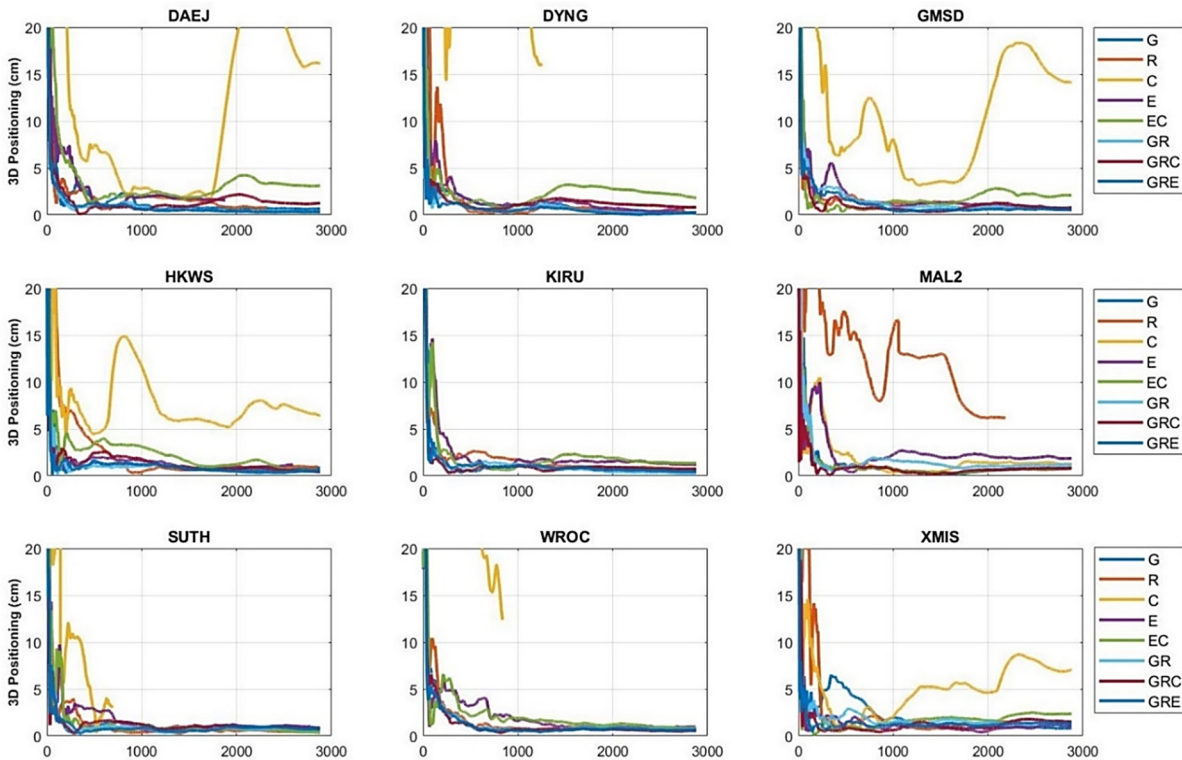
Fig. 4   3D positioning errors at IGS study sites for single system, dual system and triple GNSS PPP mode on DOY 269.

Table 5 Standard deviation of 3D positioning errors of the eight different GNSS PPP mode on DOY269 (Unit: cm).

System	IGS						
	DAEJ	DYNG	GMSD	HKWS	KIRU	MAL2	SUTH
GPS	8.43	5.73	10.65	4.67	6.10	4.72	7.71
GLONASS	9.16	11.03	14.98	21.47	16.17		14.39
BeiDou	36.00	41.92	37.11	15.49	222.77	28.51	8.30
Galileo	17.12	5.15	12.79	11.12	6.62	7.69	7.21
Galileo/BeiDou	15.36	4.88	14.87	9.15	6.48	7.49	6.02
GPS/GLONASS	6.74	6.19	9.80	4.30	5.28	4.35	7.46
GPS/GLONASS/BeiDou	7.22	5.93	10.81	3.53	4.98	4.17	7.48
GPS/GLONASS/Galileo	5.03	2.90	6.91	2.29	3.57	3.07	6.01

of DAEJ, WROC and XMIS, respectively. In addition, R-only system showed better PPP solutions than G-only PPP at KIRU and WROC in north and up component at DAEJ and DYNGIt can be inferred from Figure 3 that C-only system has higher number of visible satellites than R- only and E-only system in Asia Pacific region. This is because all geostationary (GEO) satellites of C-only system have high orbit altitude which makes the GEO satellites to be observed repeatedly during the whole day. Moreover, PPP solutions for C-only system are worse in all three components (east, north, up) at DYNG, KIRU and WROC. This is because insufficient number of available BeiDou satellites with higher PDOP values at these sites. Consequently, values of PDOP affect the positioning accuracy of the C-only PPP solutions.

In addition, with the exception of DYNG, KIRU and WROC, C-only PPP results reach about 15, 10 and 20 cm in east, north and up direction, respectively. It can be inferred from Figure 3 that positioning accuracy for combined E/C PPP is improved in all three components (east, north, up) over R-only and E- only and also in (east, north) component over G- only PPP. In addition, E/C PPP estimates show better performance than G/R PPP results at DAEJ, GMSD and XMIS in east direction and at DYNG and WROC in north and up direction. Furthermore, integration of BeiDou observations with the combined G/R PPP estimates slightly improve over G/R PPP results by only 1 – 5 mm in east, north direction and 10 – 15 mm in up direction. Moreover, adding the Galileo observations with the combined G/R PPP enhances the position accuracy in all of three position series. Difference of STD values between G/R/C and G/R/E is about 1 – 2 cm in east, north direction and 3 cm in up direction. Figure 4 shows three dimensional (3D) positioning accuracies for IGS sites on DOY 269. Table 5 presents standard deviation (STD) in three dimensions (3D) for eight GNSS PPP combinations shown in Figure 4. Analysis of Figure 4 shows that E-only and C-only PPP solutions show position variations at the beginning of epochs. Positioning solutions start to converge after several hours for both the C-only and E-only PPP. In addition, specifically in Asia Pacific region, C-only PPP show very high

variations of 3D positioning on DOY 269. Results given in Table 5 show that STD3D of single system G-only and E-only PPP are comparable. However, difference of STD3D between G-only and E-only is large at sites DAEJ and HKWS. This is because STD for DAEJ (north, up) and HKWS (east, up) component for E-only is very large as shown in Figure 3. On the other hand, 3D positioning for the combined G/R PPP better performed over combined E/C PPP results. However, results given in Table 5 show that 3D positioning accuracy improved with the integration of BeiDou observations to the E-only PPP at DYNG, SUTH and WROC on DOY 269. Moreover, PPP solutions for the triple combined G/R/E PPP best performed over G/R/C. G/R and E/C PPP results.

Figure 5 and Figure 6 show average standard deviations (STDs) and biases of east, north and up components for single system, dual system and triple system PPP mode for all IGS sites of whole ten days of data, respectively. Figure 7 shows the average STD for the horizontal (2D) and three dimensions (3D) of GPS, GLONASS, BeiDou and Galileo, GPS/GLONASS, Galileo/BeiDou, GPS/GLONASS/BeiDou and GPS/GLONASS/Galileo PPP combinations for all IGS stations. Table 6 gives the statistical summary of average positioning errors for the G–only, R–only, C–only, E–only, G/R, E/C, G/R/C and G/R/E PPP combinations.

Analysis of Figure 6 shows that average biases of C-only system is very large in east, north and up direction. In addition, biases range from -5.0 to 5.0 cm, -3.0 to 3.0 cm and -9.0 to 3.0 cm in east, north and up direction. Moreover, bias reaches to 10.0 cm in north component at DYNG and 21.0 and 11.0 cm in east and up component at KIRU, respectively. Mean bias of R-only system reaches to 0.6 and 0.7 cm at DYNG and DAEJ in east and north component, respectively. While bias reaches to 1.7, 1.6 and 1.4 cm at stations GMSD, HKWS and XMIS in up direction, respectively. On the other hand, maximum bias of G- only system reaches to 0.9, 0.5 and 1.8 cm at stations KIRU, WROC and DAEJ in east, north and up, respectively. Biases for the E-only system range - 0.1 to 1.1 cm in east direction. Mean bias of 1.1 cm
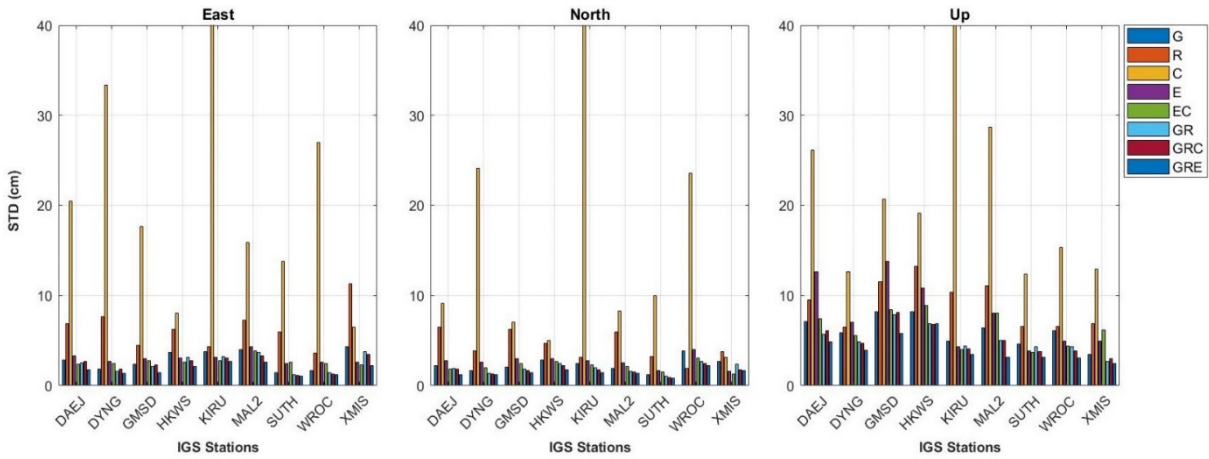
Fig.5   Bar diagram of average standard deviation (STD) in east, north and up components for eight different GNSS PPP combinations.
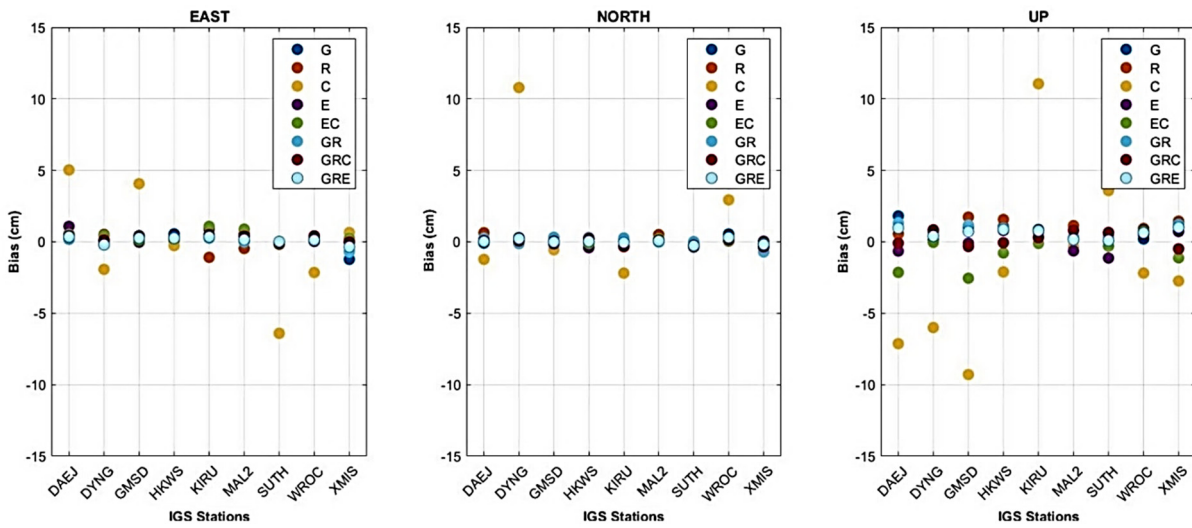
Fig.6   Biases in east, north and up components for the single, dual and triple GNSS PPP combinations.
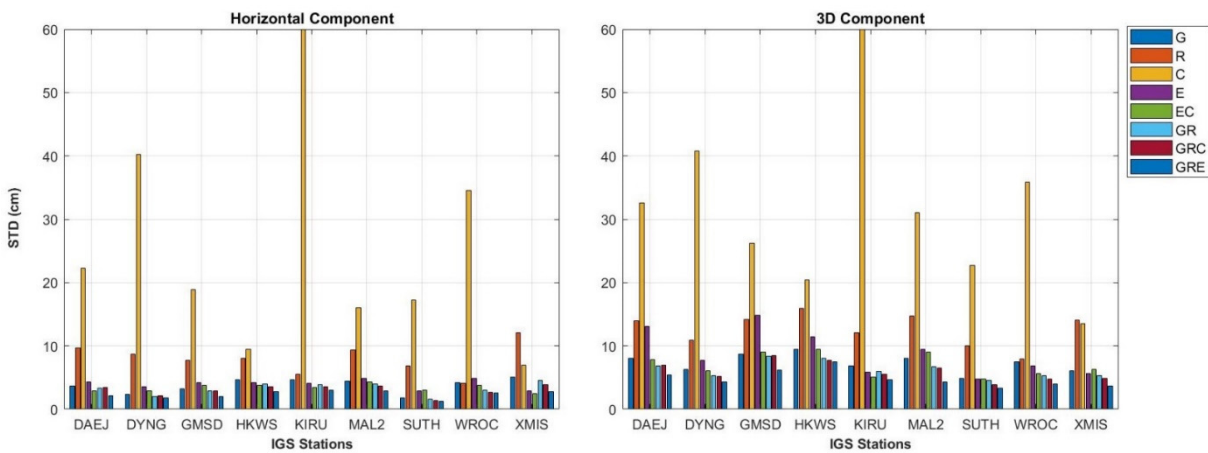
Fig.7   Statistical summary of horizontal and 3D positioning errors for single system, dual system and triple GNSS PPP combinations.

Table 6 Average biases and standard deviations of the positioning errors of the eight different GNSS PPP mode (Unit: cm).

System mode	East		North		Up		2D		3D	
	Mean	STD	Mean	STD	Mean	STD	Mean	STD	Mean	STD
GPS	0.12	2.88	0.06	2.32	0.85	6.10	1.05	3.79	2.08	7.33
GLONASS	0.05	6.40	0.03	4.36	1.02	9.12	1.71	8.00	2.81	12.65
BeiDou	2.35	23.69	1.56	15.23	-1.69	21.62	17.26	27.64	23.41	35.19
Galileo	0.31	3.01	-0.03	2.65	0.07	7.82	1.53	4.00	2.90	8.85
Galileo/BeiDou	0.40	2.68	0.01	2.14	-0.70	6.28	1.47	3.38	2.84	7.01
GPS/GLONASS	0.04	2.53	0.03	1.92	0.82	5.11	0.78	3.24	1.64	6.25
GPS/GLONASS/BeiDou	0.25	2.42	-0.03	1.70	0.23	5.04	0.89	3.02	1.73	5.97
GPS/GLONASS/Galileo	0.09	1.82	0.01	1.45	0.61	4.07	0.66	2.38	1.41	4.82

Table 7 System improvement of 3D positioning w.r.t. to single, dual and triple GNSS PPP combinations (Unit: mm).

Improvement	System mode							
	G	R	C	E	E/C	G/R	G/R/C	G/R/E
dG		7.52	39.79	1.76	/	/	/	/
dR	/		19.75	/	/	/	/	/
dE	/	5.78	37.85		/	/	/	/
dE/C	0.69	8.46	46.64	2.35		/	/	/
dG/R	1.80	10.47	48.82	3.77	1.17		/	/
dG/R/C	2.47	11.63	52.56	4.40	1.77	0.56		/
dG/R/E	5.52	17.03	66.87	8.07	4.75	3.16	2.49	

is noticeable at DAEJ (east direction). While, mean bias ranges within (-0.4 to 0.3 cm) and (-1.4 to 0.8 cm) in north and up component, respectively.

It can be illustrated from Figure 6 that mean bias for combined dual system E/C reaches to 1.1 and 0.9 cm at KIRU and MAL2 in east component, respectively. While, bias ranges within -0.3 to 0.2 and -2.5 to 0.7 cm in north and up component, respectively.

Moreover, mean bias for the combined triple G/R/C PPP mode is comparatively large than the G/R/E PPP biases in east and north components. However, combined G/R/E PPP mean bias at WROC reaches to 0.30 cm in north component than G/R/C PPP which is 0.17 cm. Furthermore, mean bias of up component for the G/R/E PPP reaches to 1.00 and 0.95 cm in comparison with G/R/C PPP mean bias which is -0.49 and -0.11 cm at stations XMIS and DAEJ, respectively.

It can be noticed from Figure 7 that horizontal positioning for the G-only PPP is enhanced at all IGS stations than R-only, C-only and E-only PPP estimates. However, at XMIS, horizontal component for G-only PPP reaches to 5.13 cm which is comparatively large than E-only PPP system. In addition, as results given in Table 6, difference of STD of horizontal component between G-only and E-only is 2.0 mm.

Analysis of Figure 7 and results given in Table 6 show that with the addition of BeiDou observation to the E-only PPP horizontal positioning further improves and average 2D component reaches to

3.38 cm for the combined E/C PPP. In addition, horizontal positioning error for the combined E/C PPP is reduced specifically in Asia Pacific region than the G/R PPP mode. Furthermore, triple combined system G/R/C PPP and G/R/E PPP further enhances the horizontal positioning. In addition, difference of STD between horizontal component for G/R/C and G/R/E PPP is 6 – 7 mm. Table 7 shows the improvement of GNSS system with respect to (w.r.t) single (G-only, R- only, E-only, C-only), dual system (E/C, G/R) and triple combine system (G/R/C and G/R/E/) PPP. Results given in Table 7 are obtained from the average of daily IGS sites from whole ten days of datasets. Results given in Table 6 and Table 7 show that 3D positioning accuracy for G-only system show better PPP performance and reaches to 7.33 cm as compare with the R-only, C-only and E-only PPP results. In addition, E-only PPP show an improvement of 3D component over R-only and C-only PPP. However, E- only PPP show an insignificant improvement over R-only PPP at GMSD site. This is because vertical component of E-only PPP reaches to 13.81 cm at this station. Moreover, combined G/R PPP mode show an average improvement of 11.73 % over E/C PPP. On the other hand, with the addition of BeiDou observation to the combine G/R PPP reach to 5.97 cm. In addition, 3D positioning accuracy of G/R/C can be improved by 5.59 % and 17.72 % over G/R and E/C PPP solutions, respectively. Moreover, 3D component for combine triple system G/R/E reaches to 4.82 cm, which show an improvement of 47.53 %, 31.56 % and 24.90 % over E/C, G/R and G/R/C PPP results.
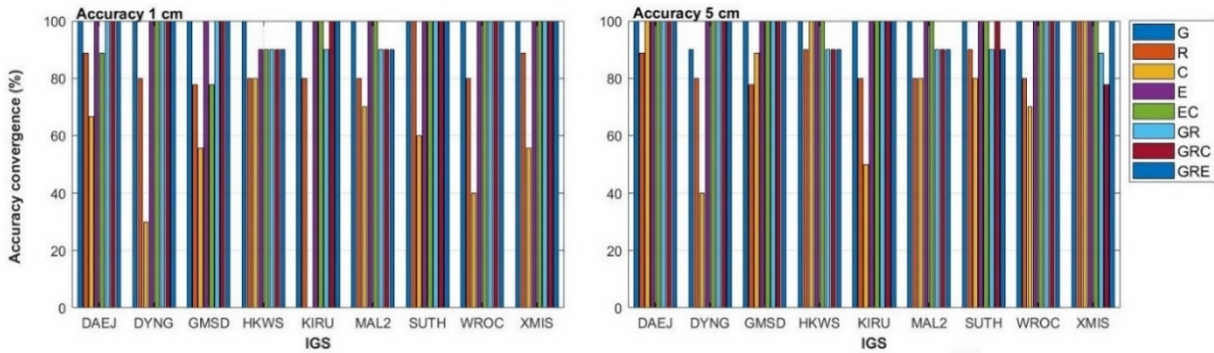
Fig. 8   Percentage of daily convergence of single system (G, R, C, E), dual system (EC, GR), and triple system (GRC, GRE) PPP mode for positioning accuracy better than 1 cm and 5 cm.
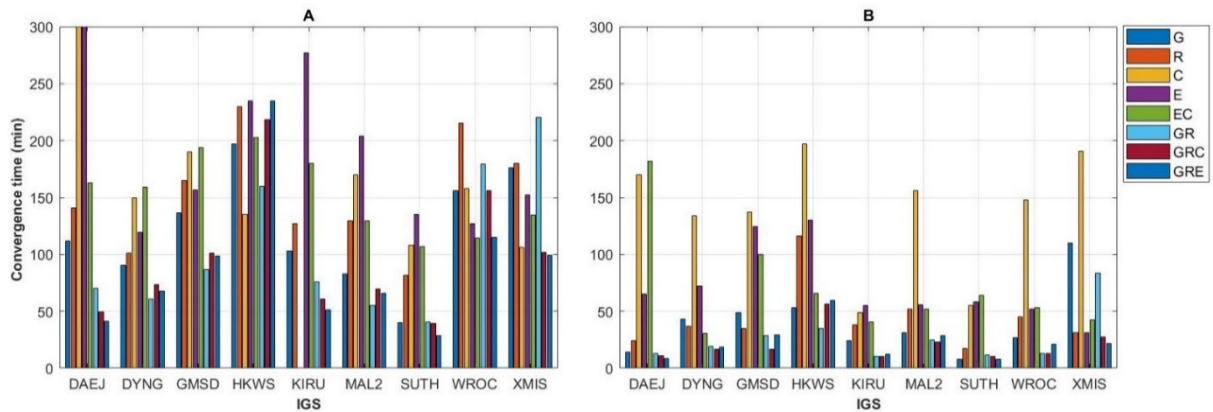
Fig. 9   Average convergence time of single system (G, R, C, E), dual system (EC, GR), and triple system (GRC, GRE) PPP at each IGS. (Letter: A = Accuracy for 1.0 cm, B = Accuracy for 5.0 cm).

5. ANALYSIS OF CONVERGENCE TIME

In this section convergence time length of GPS, GLONASS, Galileo, BeiDou, Galileo/BeiDou, GPS/GLONASS, GPS/GLONASS/BeiDou and GPS/GLONASS/Galileo PPP mode is analysed and evaluated. Convergence time depends on visibility of number of available satellites, geometry of satellites, environment conditions of the reception of the GNSS observations (Cai and Gao, 2013). For the analysis of convergence time, predefined threshold value is adopted in order to evaluate the convergence length. The solution is considered as converged if the 3D positioning error has been suppressed lower than the threshold value of 1.0 cm or 5.0 cm for at least twenty epochs. Two different positioning accuracy (1 and 5 cm) is adopted for the single, dual and triple GNSS PPP mode only because some geodetic applications has minimum threshold set ($\geq$ 5.0 cm) to achieve desired accuracy level. Figure 8 presents average percentage of convergence time during ten days of data observations for G–only, R–only, C–only and E– only, combined dual system G/R and E/C, triple system G/R/C and G/R/E PPP mode. Figure 9 shows the convergent session's length of 3D positioning accuracy for the eight different PPP combinations at all IGS sites to achieve positioning accuracy level of 1.0 cm and 5.0 cm. Figure 10 presents the bar graph

of average convergence time for GNSS system mode of all IGS from whole ten days of datasets. It can be demonstrated from Figure 8 that among single system, average percentage of daily convergence time for R- only and C-only system is not uniform to achieve accuracy for both the 1 and 5 cm.

However, combine three system G/R/C PPP show fastest convergence speed and takes only 20.6 min than the G/R/E PPP to converge accuracy better than 5.0 cm. Table 8 outlines the standard
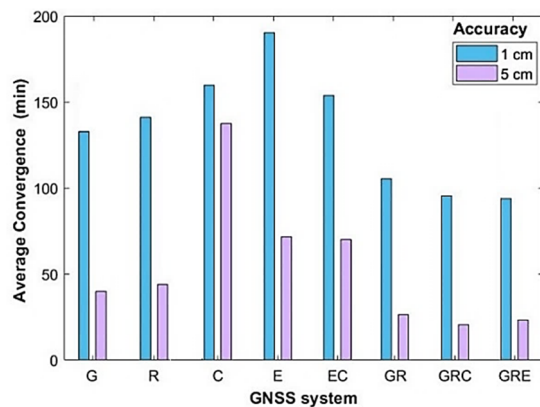
Fig. 10   Bar diagram of average convergence time for the GNSS system.

Table 8 Standard Deviation of average convergence time for single, dual and triple GNSS PPP solutions.

System mode	Convergence time (min)	
	1.0 cm	5.0 cm
GPS	98.27	29.71
GLONASS	102.41	40.37
BeiDou	126.10	149.61
Galileo	141.58	64.06
Galileo/BeiDou	121.17	67.26
GPS/GLONASS	85.24	21,60
GPS/GLONASS/BeiDou	80.61	20.81
GPS/GLONASS/Galileo	74.92	20.99

deviation (STD) of average convergence time for eight GNSS PPP solutions. It can be noticed from results given in Table 8 that convergence time length is short of G-only PPP than the R-only, E-only and C-only convergent sessions. Convergence time for the G-only can be improved by 45.55 %, 81.22 % and 70.10 % over R-only, C-only and E-only convergence time length. For the R-only convergence time, STD of average time show an improvement of 40.44 % and 22.0 % over C-only and E-only time sessions. However, insignificant improvement notices for R- only over E-only PPP at stations GMSD, SUTH and XMIS. In addition, convergence speed for E-only is significantly increases over C-only at stations DAEJ, DYNG, SUTH and WROC.

Results given in Table 8 illustrate that G/R PPP take 85.24 and 21.06 min to converge accuracy level of 1.0 and 5.0 cm, respectively. Moreover, combine G/R PPP convergence time show an improvement of 56.46 % over G-only time length. The contribution of BeiDou to reducing the convergence time of the combine G/R PPP can be improved by 71.92 % and 27.53 % over G-only and combine G/R PPP convergence time, respectively. Furthermore, standard deviation (STD) values demonstrate that with the addition of Galileo observations to the combine G/R convergent sessions, average convergent performance of the combined G/R/E PPP is improved and steadier to achieve the 3D positioning accuracy level of 1.0 and 5.0 cm. In addition, G/R/E PPP convergence speed shows an improvement of 33.79 % and 20.06 % over convergent sessions of G/R and G/R/C PPP results. Furthermore, to achieve accuracy level of 5.0 cm, combine three systems G/R/C PPP convergence time reduces to 20.81 min than the 20.99 min for the G/R/E convergent time length.

6. CONCLUSION

To combine observations from multi GNSS system further increases the PPP performance and GNSS positioning accuracy. In this study, undifferenced and uncombined observation model (UDUC) is used in order to evaluate and comparative analyse the positioning accuracy of GPS, GLONASS, BeiDou, Galileo, Galileo/BeiDou,

GPS/GLONASS, GPS/GLONASS/BeiDou and GPS/GLONASS/Galileo PPP system mode. Recently available multi-GNSS open software package utilizes for post-processing the static PPP experiment tests. Ten days of dataset from nine IGS reference sites are adopted for eight different GNSS PPP scenarios.

Results demonstrate that PPP solutions of GPS- only show an improvement in east, north and up components over GLONASS-only, BeiDou-only and Galileo-only PPP solutions.GPS PPP solutions reach to 2.88, 2.32 and 6.10 cm in east north and up components, respectively. Difference of standard deviation (STD) values between GPS and GLONASS PPP results is 4, 3 and 2 cm, in east, north and up direction, respectively. Positioning accuracy of Galileo-only PPP shows a significant improvement over GLONASS-only and BeiDou-only PPP. PPP estimates for Galileo are 3.01, 2.65 and 7.82 cm in east, north and up, respectively. Furthermore, it also notice that PPP solutions of BeiDou-only PPP show better estimates in Asia-Pacific region only. BeiDou only PPP results reach to 15, 10 and 20 cm in east, north and up direction in Asia Pacific, respectively. PPP solutions for BeiDou only are still constrained by the poor satellite geometry and the limited accuracy of the orbit and clock products availability, specifically BeiDou GEO (Geostationary Earth Orbit). Addition of GLONASS observations to the GPS-only solutions further enhances the PPP performance. GPS/GLONASS PPP results reach to 2.53, 1.92 and 5.11 cm in east, north and up components compare with combined Galileo/BeiDou PPP solutions. However, daily positioning errors for combine GPS/GLONASS PPP at some IGS sites are relatively high than the Galileo/BeiDou PPP, which may be related that by the addition of GLONASS observations also increases the number of parameters to be estimated. Horizontal component for combine Galileo/BeiDou PPP and GPS/GLONASS PPP solutions reach to 3.24 and 3.02 cm, respectively. While, difference of STD between horizontal component for GPS/GLONASS/BeiDou and GPS/GLONASS/Galileo PPP is 6 – 7 mm. 3D positioning accuracy for GPS-only system show better PPP performance and reaches to 7.33 cm Moreover, combined GPS/GLONASS PPP mode show an average improvement of 11.73 % over Galileo/BeiDou PPP results. On the other hand, with the addition of BeiDou observations to the combine GPS/GLONASS PPP STD3D reach to 5.97 cm. 3D positioning accuracy of GPS/GLONASS/BeiDou can be improved by 5.59 % and 17.72 % over GPS/GLONASS and Galileo/BeiDou PPP solutions, respectively. Moreover, 3D component for combine triple system GPS/GLONASS/Galileo shows an improvement of 47.53 %, 31.56 % and 24.90 % over Galileo/BeiDou PPP, GPS/GLONASS PPP and GPS/GLONASS/BeiDou PPP, respectively.

Results analysis of average convergence time show that GPS-only converges fastest out of

GLONASS, BeiDou, Galileo PPP combinations mode to achieve 3D positioning accuracy level of 1.0 and 5.0 cm. Average convergence time of. GPS-only PPP takes 132 min to achieve accuracy level of 1 cm. Comparison with BeiDou-only PPP and Galileo PPP, convergence time for combine Galileo/BeiDou PPP shortens and takes 153.77 min and 70.0 min to achieve accuracy level of 1.0 and 5.0 cm, respectively. However, convergence speed for the combine Galileo/BeiDou PPP is not significantly improves as compare with the dual system GPS/GLONASS convergent sessions length. This is because different orbital types of BeiDou system (MEO, GEO and IGSO). In addition, slower changing geometry of the GEO/IGSO satellites than the MEO orbital type satellites (Liu et al., 2017; Zhao et al., 2015). STD values of convergence time for the combine GPS/GLONASS PPP show an improvement of 56.46% over GPS-only time length. The convergence time of the combine GPS/GLONASS/BeiDou PPP can be improved by 71.92 % and 27.53 % over GPS-only and combine GPS/GLONASS PPP convergence time, respectively. Furthermore, STD values of average convergence speed of the combined GPS/GLONASS/Galileo PPP show an improvement of 33.79 % and 20.06 % over GPS/GLONASS PPP and GPS/GLONASS/BeiDou PPP, respectively.

With the continuous development of BeiDous and Galileo system (Kiliszek and Kroszczyński, 2020) and multiple frequencies available, it would be of great significance to enhance the stability of the multi GNSS system and shorten the convergence time (Ogutcu, 2020). Therefore, it is required to conduct further research on multi-GNSS combination.

ACKNOWLEDGEMENT

REFERENCES

Acheampong, A.A., Fosu, C., Amekudzi, L.K. and Kaas, E.: 2016, Comparison of precipitable water over Ghana using GPS signals and reanalysis products. J. Geod. Sci. 5, 163–170. DOI: 10.1515/jogs-2015-0016

Afifi, A. and El-Rabbany, A.: 2016, Precise point positioning using triple GNSS constellations in various modes. Sensors, 16, 6, 779. DOI: 10.3390/s16060779

Bahadur, B. and Nohutcu, M.: 2018, PPPH: a MATLAB-based software for multi-GNSS precise point positioning analysis. GPS Solut., 22, 4, 113. DOI: 10.1007/s10291-018-0777-z

Cai, C. and Gao, Y.: 2013, Modeling and assessment of combined GPS / GLONASS precise point positioning. GPS Solut., 17, 2, 223–236. DOI: 10.1007/s10291-012-0273-9

Cai, C. and Gao, Y.: 2007, Precise point positioning using combined GPS and GLONASS observations. J. Glob. Position. Syst., 6, 1, 13–22. DOI: 10.5081/jgps.6.1.13

Capilla, R.M., Berné, J.L., Martín, A. and Rodrigo, R.: 2016, Simulation case study of deformations and landslides using real-time GNSS precise point positioning technique. Geomatics, Nat. Hazards Risk, 7, 6, 1856–1873. DOI: 10.1080/19475705.2015.1137243

Choy, S., Zhang, S., Lahaye, F. and Héroux, P.: 2013, A comparison between GPS-only and combined GPS+GLONASS Precise Point Positioning. J. Spat. Sci., 58, 2, 169–190. DOI: 10.1080/14498596.2013.808164

Dach, R., Brockmann, E., Schaer, S., Beutler, G., Meindl, M., Prange, L., Bock, H., Jäggi, A. and Ostini, L.: 2009, GNSS processing at CODE: Status report. J. Geod., 83, 353–365. DOI: 10.1007/s00190-008-0281-2

Dong, Z. and Jin, S.: 2018, 3-D water vapor tomography in Wuhan from GPS, BDS and GLONASS observations. Remote Sens., 10, 1, 62. DOI: 10.3390/rs10010062

Hein, G.W.: 2020, Status, perspectives and trends of satellite navigation. Satell. Navig., 1, 22, 1–12. DOI: 10.1186/s43020-020-00023-x

Herring, T.A., King, R.W., Floyd, M.A. and McClusky, S.C.: 2015, Introduction to GAMIT/GLOBK. Release 10.6, Mass. Inst. of Technol., Cambridge, 1–50.

Sanz Subirana, J., Juan Zornoza, J.M. and Hernandéz-Pajares, M.: 2013, GNSS Data Processing, Volume II: Laboratory Exercises, European Space Agency.

Kiliszek, D. and Kroszczyński, K.: 2020, Performance of the precise point positioning method along with the development of GPS, GLONASS and Galileo systems. Measurement, 164, 108009. DOI: 10.1016/j.measurement.2020.108009

Kouba, J. and Héroux, P.: 2001, Precise point positioning using IGS orbit and clock products. GPS Solut., 5, 12–28. DOI: 10.1007/PL00012883

Li, R., Zheng, S., Wang, E., Chen, J., Feng, S., Wang, D. and Dai, L.: 2020, Advances in BeiDou Navigation Satellite System (BDS) and satellite navigation augmentation technologies. Satell. Navig., 1, 1–23. DOI: 10.1186/s43020-020-00010-2

Li, X., Dick, G., Lu, C., Ge, M., Nilsson, T., Ning, T., Wickert, J. and Schuh, H.: 2015, Multi-GNSS meteorology: Real-time retrieving of atmospheric water vapor from BeiDou, Galileo, GLONASS, and GPS observations. IEEE Trans. Geosci. Remote Sens., 53, 12, 6385–6393. 10.1109/TGRS.2015.2438395

Liu, G., Zhang, X. and Li, P.: 2019, Improving the performance of Galileo uncombined precise point positioning ambiguity resolution using triple-frequency observations. Remote Sens., 11, 341. DOI: 10.3390/rs11030341

Liu, T., Yuan, Y., Zhang, B., Wang, N., Tan, B. and Chen, Y.: 2017, Multi-GNSS precise point positioning (MGPPP) using raw observations. J. Geod., 91, 253–268. DOI: 10.1007/s00190-016-0960-3

Liu, X., Chen, H., Jiang, W., Xi, R., Zhao, W., Song, C. and Zhou, X.: 2019, Modeling and assessment of GPS/Galileo/BDS precise point positioning with

ambiguity resolution. Remote Sens., 11, 22, 2693. DOI: 10.3390/rs11222693

Lou, Y., Zheng, F., Gu, S., Wang, C., Guo, H. and Feng, Y.: 2016, Multi-GNSS precise point positioning with raw single-frequency and dual-frequency measurement models. GPS Solut., 20, 849–862. DOI: 10.1007/s10291-015-0495-8

Malik, J.S.: 2020, Performance analysis of static precise point positioning using open-source GAMP, Artif. Satell., 55, 2, 41–60. DOI: 10.2478/arsa-2020-0004

Malik, J.S., Jingrui, Z. and Naqvi, N.A.: 2017, Soil moisture content estimation using GNSS reflectometry (GNSS-R). 5th Int. Conf. Aerosp. Sci. Eng (ICASE 2017), 1–9. DOI: 10.1109/ICASE.2017.8374264

Martín, A., Anquela, A.B., Capilla, R. and Berné, J.L.: 2011. PPP technique analysis based on time convergence, repeatability, IGS products, different software processing, and GPS+GLONASS constellation. J. Surv. Eng., 137, 3, 99–108. DOI: 10.1061/(ASCE)SU.1943-5428.0000047

Ogutcu, S.: 2020, Assessing the contribution of Galileo to GPS+GLONASS PPP: Towards full operational capability. Measurement, 151, 107143. DOI: 10.1016/j.measurement.2019.107143

Pan, L., Zhang, X., Li, Xingxing, Li, Xin, Lu, C., Liu, J., and Wang, Q.: 2019, Satellite availability and point positioning accuracy evaluation on a global scale for integration of GPS, GLONASS, BeiDou and Galileo. Adv. Sp. Res., 63, 9, 2696–2710. DOI: 10.1016/j.asr.2017.07.029

Saastamoinen, J.: 1972, Contributions to the theory of atmospheric refraction. Bull. Geodesique, 46, 279–298. DOI: 10.1007/BF02521844

Salazar, D., Hernandez-Pajares, M., Juan, J.M. and Sanz, J.: 2010, GNSS data management and processing with the GPSTk. GPS Solut., 14, 293–299. DOI: 10.1007/s10291-009-0149-9

Shi, C., Zhao, Q.L, Li, M., Tang, W.M., Hu, Z.G., Lou, Y.D., Zhang, H.P., Niu, X.J. and Liu, J.N.: 2012, Precise orbit determination of Beidou satellites with precise positioning. Sci. China Earth Sci., 55, 1079–1086. DOI: 10.1007/s11430-012-4446-8

Tadokoro, K., Ikuta, R., Watanabe, T., Ando, M., Okuda, T., Nagai, S., Yasuda, K. and Sakata, T.: 2012, Interseismic seafloor crustal deformation immediately above the source region of anticipated megathrust earthquake along the Nankai Trough, Japan. Geophys. Res. Lett., 39, 10, 1–5. DOI: 10.1029/2012GL051696

Wang, G.Q.: 2013, Millimeter-accuracy GPS landslide monitoring using Precise Point Positioning with Single Receiver Phase Ambiguity (PPP-SRPA) resolution: a case study in Puerto Rico. J. Geod. Sci., 3, 1, 22–31. DOI: 10.2478/jogs-2013-0001

Wang, M., Chai, H. and Li, Y.: 2017, Performance analysis of BDS/GPS precise point positioning with undifferenced ambiguity resolution. Adv. Sp. Res., 60, 12, 2581–2595. DOI: 10.1016/j.asr.2017.01.045

Xia, F., Ye, S., Xia, P., Zhao, L., Jiang, N., Chen, D. and Hu, G.: 2019, Assessing the latest performance of Galileo-only PPP and the contribution of Galileo to Multi-GNSS PPP. Adv. Sp. Res., 63, 9, 2784–2795. DOI: 10.1016/j.asr.2018.06.008

Yigit, C.O., Gikas, V., Alcay, S. and Ceylan, A.: 2014, Performance evaluation of short to long term GPS, GLONASS and GPS/GLONASS postprocessed PPP. Surv. Rev., 46, 336, 155–166. DOI: 10.1179/1752270613Y.0000000068

Zhao, Q., Wang, C., Guo, J. and Liu, X.: 2015, Assessment of the contribution of BeiDou GEO, IGSO, and MEO satellites to PPP in Asia-Pacific region. Sensors, 15, 12, 29970–29983. DOI: 10.3390/s151229780

Zhao, X., Wang, S., Liu, C., Ou, J. and Yu, X.: 2017, Assessing the performance of multi-GNSS precise point positioning in Asia-Pacific region. Surv. Rev., 49, 354, 186–196. DOI: 10.1080/00396265.2016.1151576

Zhou, F., Dong, D., Ge, M., Li, P., Wickert, J. and Schuh, H.: 2018a, Simultaneous estimation of GLONASS pseudorange inter-frequency biases in precise point positioning using undifferenced and uncombined observations. GPS Solut., 22, 1–14. DOI: 10.1007/s10291-017-0685-7

Zhou, F., Dong, D., Li, W., Jiang, X., Wickert, J. and Schuh, H.: 2018b, GAMP: An open-source software of multi-GNSS precise point positioning using undifferenced and uncombined observations. GPS Solut., 22, 1, 1–10. DOI: 10.1007/s10291-018-0699-9

Zumberge, J.F., Heftin, M.B., Jefferson, D.C. and Watkins, M.M.: 1997, Precise point positioning for the efficient and robust analysis of GPS data from large networks. J. Geophys. Res., 102, B3, 5005–5017. DOI: 10.1029/96JB03860